Journal of ELECTRONIC MATERIALS, Vol. 43, No. 2, 2014
DOI: 10.1007/s11664-013-2900-9

Effects of Heat-Treatment Temperature on the Microstructure, Electrical and Dielectric Properties of M-Type Hexaferrites

IHSAN ALI,[1,3] M.U. ISLAM,[1] M.S. AWAN,[2,4] and MUKHTAR AHMAD[1]

1.—Department of Physics, Bahauddin Zakariya University, Multan 60800, Pakistan. 2.—Center for Micro and Nano Devices, Department of Physics, COMSATS Institute of Information Technology, Islamabad, Pakistan. 3.—e-mail: ihsanali.ap@gmail.com. 4.—e-mail: muislampk@yahoo.com

M-type hexaferrite $BaCr_xGa_xFe_{12-2x}O_{19}$ ($x = 0.2$) powders have been synthesized by use of a sol–gel autocombustion method. The powder samples were pressed into 12-mm-diameter pellets by cold isostatic pressing at 2000 bar then heat treated at 700°C, 800°C, 900°C, and 1000°C. X-ray diffraction patterns of the powder sample heat treated at 1000°C confirmed formation of the pure M-type hexaferrite phase. The electrical resistivity at room temperature was significantly enhanced by increasing the temperature of heat treatment and approached 5.84×10^9 Ω cm for the sample heat treated at 1000°C. Dielectric constant and dielectric loss tangent decreased whereas conductivity increased with increasing applied field frequency in the range 1 MHz–3 GHz. The dielectric properties and ac conductivity were explained on the basis of space charge polarization in accordance with the Maxwell–Wagner two-layer model and Koop's phenomenological theory. The single-phase synthesized materials may be useful for high-frequency applications, for example reduction of eddy current losses and radar absorbing waves.

Key words: Hexaferrites, microstructure, heat treatment, dielectric properties

INTRODUCTION

Ferrites are useful electrical materials, because of their high resistivity and low loss behavior, with many technological applications over a wide range of frequencies. They are used in home appliances, electronic products, communication equipment, data-processing devices, radio, television, microwave and satellite communications. Advantages of ferrites include their greater efficiency and lower cost than other materials.[1] In recent years there has been much interest in the properties of nano-sized ferrite particles, because of their importance in the fundamental understanding of physical processes and their many proposed technological applications. The physical properties of nano-materials are predominantly determined by the grain boundaries rather than by the grains.[2] The electrical properties of nano ferrites are greatly affected when particle size approaches the critical size below which each particle is treated as a single domain.[3] Because communication and electronic systems are moving to higher working frequencies, spinel ferrites seem to fall short on new demands, because of intrinsic restrictions imposed by the occurrence of their natural ferromagnetic resonance up to 1 GHz. Technological progress has revealed the potential of hexaferrites to replace spinel ferrites in applications containing ferrite devices and operating at microwave frequencies as microwave absorbers.[4] Hexaferrites have been used as permanent magnets for a long time and are still a topic of research because of their good properties in microwave devices and magneto-optic or perpendicular recording media. M-type compounds ($MFe_{12}O_{19}$; M = Ba, Sr) are the most studied among the different stable phases.[5]

Sol–gel autocombustion is of interest because of its use of heat released from the reactions of fuels (hydrocarbon species from chelating agents) and oxidants (nitrate radicals) for rapid formation of

(Received November 12, 2012; accepted August 29, 2013; published online November 21, 2013)

nano-powders.[6] The main advantages of sol–gel autocombustion over the ceramic route are excellent homogeneity, nanosized granulation, enhanced reactivity (lower heat-treatment temperatures), and control of grain size by subsequent heat treatment.[7] Average grain size tends to decrease regularly with increasing Cr content, because substitution of Cr inhibits grain growth. This results in enhancement of coercivity.[8] Substitution of Ga for Fe results in an increase in coercivity, which is attributed to attenuation of magnetic exchange coupling.[9]

The purpose of this work was to study the effects of different heat-treatment temperatures (700°C, 800°C, 900°C, and 1000°C) on the microstructure, electrical and dielectric properties of gallium–chromium-substituted M-type barium hexaferrite $BaCr_xGa_xFe_{12-2x}O_{19}$ ($x = 0.2$) produced by the sol–gel autocombustion method.

EXPERIMENTAL PROCEDURES

M-type hexaferrite $BaCr_xGa_xFe_{12-2x}O_{19}$ ($x = 0.2$) was synthesized by use of the sol–gel autocombustion method. The procedure, illustrated in Fig. 1, was adapted from our previous research.[10–12] Stoichiometric amounts of the starting materials $Ba(NO_3)_2$ (99%, Sigma–Aldrich), $Fe(NO_3)_3{\cdot}9H_2O$ (98%, Applichem), $Cr(NO_3)_3.4H_2O$ (99%, Sigma–Aldrich), and $Ga(NO_3)_3{\cdot}4H_2O$ (99.9%, Sigma–Aldrich) were dissolved in 500 mL de-ionized water in a 1000-mL Pyrex beaker. Citric acid was added to the solution (metal-to-citric acid molar ratio 1:1) then the pH was adjusted to 7 by addition of ammonia solution (Riedel–de Haën, 33%). This solution was evaporated at a constant temperature of approximately 80°C with constant stirring on a hot plate magnetic stirrer until it turned into a viscous gel. The temperature of the hot plate magnetic stirrer was then increased to approximately 200°C for ignition of the gel. The gel was burnt to a dendritic and brittle powder with citric acid as reductant and nitrate as oxidant. The as-prepared powders were reddish–brown and voluminous. The powder samples were pressed into high density 12-mm-diameter pellets by cold isostatic pressing (CIP). Water was used as medium for pressing the as-prepared powder into pellets. In the CIP technique, pressure was applied from different directions to achieve more uniform compaction and better shape than uniaxial pressing. The powder sample was enclosed in a rubber sheath and immersed in water, which transmits the pressure uniformly to the powder. First, pressing of the powder samples was performed uniaxially; for further densification they were then subjected to isostatic pressing at a pressure of 2000 bar. Samples in the pellet or powder form were placed in ceramic boats and individually heat treated for 4 h at 700°C, 800°C, 900°C, and 1000°C in a Protherm Turky digitally controlled temperature-programmed tube furnace, in an air environment, at a heating rate of 30° min^{-1}, to convert the samples into the M-type hexagonal phase.

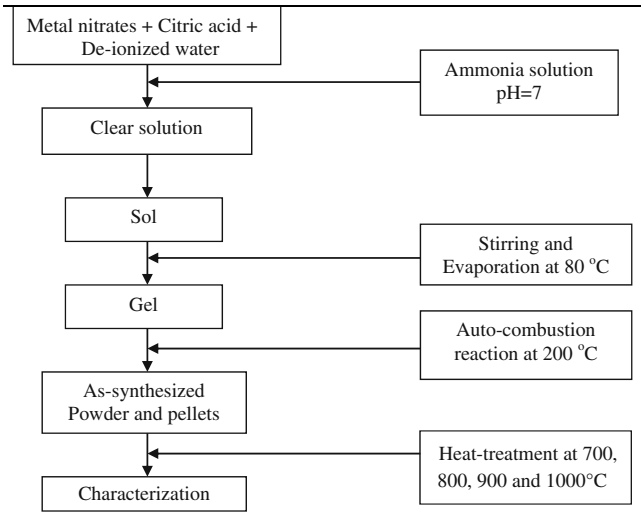

Fig. 1. Flow-chart for synthesis of M-type hexaferrite $BaCr_xGa_xFe_{12-2x}O_{19}$ ($x = 0.2$) powder.

X-ray diffraction (XRD) analysis was performed by use of an X'Pert PRO PANAlytical x-ray diffractometer with a Cu Kα radiation source of wavelength $\lambda = 1.5406$ Å. The diffraction intensity was measured with scan steps of 0.02° for a 2θ range from 10° to 80°. The surface morphology and microstructure of the sintered powders were studied by use of an Hitachi S4160 scanning electron microscope (SEM). Elemental composition was determined by energy-dispersive x-ray spectroscopy (EDXS) with an Horiba MESA-500.DC electrical resistivity was measured by the two-point probe method using the Keithley model 2400 source meter. The dielectric properties of the synthesized materials at room temperature were measured in the frequency range 1 MHz–3 GHz by use of an Agilent model E4991A RF impedance analyzer.

RESULTS AND DISCUSSION

Thermal Analysis

Dehydration, decomposition of residual organic groups, and phase formation of hexaferrites occurred during heat treatment of as-prepared samples. Differential scanning calorimetric (DSC) and thermogravimetric (TG) analysis of the as-prepared powder sample, in a platinum crucible, were performed up to 1000°C at a heating rate of 10° min^{-1}, in argon gas, to study weight loss and transformation of different phases during heat treatment. Figure 2 shows the DSC–DDSC and TG curves of as-prepared powder sample $BaCr_xGa_xFe_{12-2x}O_{19}$ ($x = 0.2$). The DSC curve contains different peaks at approximately 211.0°C, 386.0°C, 601.1°C, 782.1°C, 851.1°C, and 1003.8°C. The endothermic peak at approximately 211.0°C can be attributed to loss of free and hydrated water and

removal of CO_2.[13,14] The exothermic peak at approximately 386.0°C may be ascribed to decomposition of remaining un-reacted citric acid.[10] The exothermic peak at approximately 601.1°C may be attributed to formation of metal oxides from hydroxides. The interaction between very reactive Ba^{2+} ions and CO or CO_2 liberated by decomposition of citric acid leads to formation of $BaCO_3$. The endothermic peak at approximately 782.1°C can be attributed to decarboxylation of $BaCO_3$ formed during combustion, and to simultaneous formation of mono-ferrite.[13] The reaction between mono-ferrite and iron oxide (α-Fe_2O_3) leads to the formation of barium hexaferrites. The exothermic peak at approximately 851.1°C can be attributed to a solid-state reaction leading to gradual formation of barium hexaferrite.[14] The exothermic peak at approximately 1003.8°C can be ascribed to formation of the M-type hexaferrite phase.[15] Figure 2 shows the gradual weight-loss which results from transformation of the different phases during heat treatment.

XRD Analysis

Figure 3 shows the XRD patterns of M-type hexaferrite $BaCr_xGa_xFe_{12-2x}O_{19}$ (x = 0.2) powder samples heat treated at 700°C, 800°C, 900°C, and 1000°C. The d values of all detected peaks were compared with the standard patterns on JCPDS cards (00-043-0002) of M-type barium hexaferrite. Patterns obtained from samples heat treated at 700°C, 800°C, and 900°C contained peaks related to the M-type hexagonal major phase; a single peak of α-Fe_2O_3 with a 2θ value of 33.80° was also observed. However, calcination at 1000°C resulted in complete disappearance of the α-Fe_2O_3 phase, and the XRD patterns were indicative of a single BaM-type phase for this sample. Sintering temperature and time have significant effect on the crystal structure of materials. Diffraction peaks with 2θ values 30.4°, 32.3°, 34.2°, 35.3°, 37.2°, 40.4°, 42.6°, 55.2°, 56.7°, 63.2°, and 72.6° arise from the diffraction planes (1 1 0), (1 0 7), (0 0 2), (1 0 8), (1 1 6), (2 0 5), (2 0 6), (0 0 14), (1 1 12), (2 0 13), and (3 1 7). These diffraction planes are indicative of pure M-type hexaferrite phase of the sample heat treated at 1000°C. It has previously been observed that increasing the treatment temperature is useful for eliminating secondary phases and forming the pure hexaferrite phase; our results are in good agreement with these results.[7] Calcination of hexaferrite within the range 1000–1100°C results in improved crystallinity and complete reaction of the constituents.[16]

Microstructure

The average crystallite size (D) of the synthesized samples was calculated by using the Scherrer formula:

$$D = \frac{K\lambda}{\beta \cos\theta}, \quad (1)$$

where λ is the x-ray wavelength, β the peak width at half height, θ the Bragg angle, and the value of the shape factor, K, for hexaferrites is 0.89.[17] The average crystallite size determined from the most intense peak was found to be in the range 44–73 nm, as listed in Table I. It also seems that the most intense peak is the (002) reflection. This means that the crystallite size reported is related solely to the crystallite size along the c-axis of the structure. It was observed that the crystallite size of the sample increased gradually with increasing

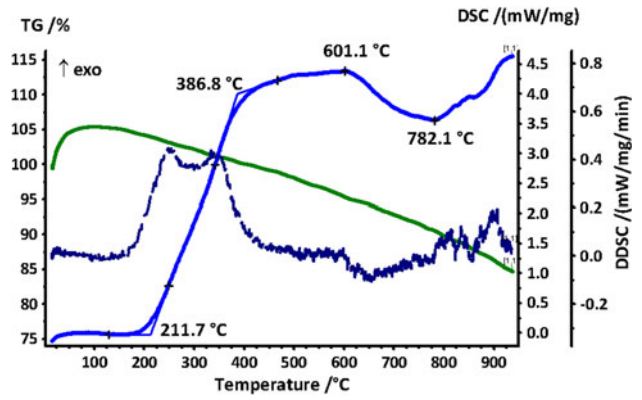

Fig. 2. DSC–DDSC and TG curves of as-prepared powder sample $BaCr_xGa_xFe_{12-2x}O_{19}$ (x = 0.2).

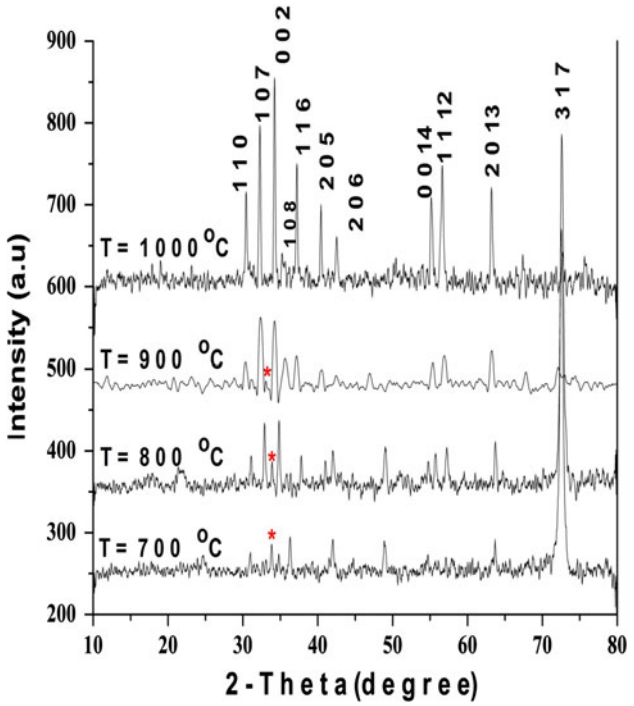

Fig. 3. XRD patterns of M-type hexaferrite $BaCr_xGa_xFe_{12-2x}O_{19}$ (x = 0.2) powder sample heat treated at different temperatures. The peaks for which h k l values are given arise from barium hexaferrites. *Asterisks* indicate the α-Fe_2O_3 phase.

Table I. Crystallite size (D), density (d_b), AC electrical conductivity (σ_{AC}), DC electrical resistivity (ρ_{RT}), dielectric constant (ε'), and dielectric loss tangent (tan δ) of M-type hexaferrites $BaCr_xGa_xFe_{12-2x}O_{19}$ (x = 0.2)

Property	700°C	800°C	900°C	1000°C
D (nm) ± 1	44	57	69	73
D_b (g cm^{-3}) ± 0.01	4.25	4.44	4.51	4.49
$\sigma_{AC} \times 10^{-3}$ (Ω cm)$^{-1}$ at 500 MHz	1.60	1.66	3.26	27.0
$\rho_{RT} \times 10^{+09}$ (Ω cm) at 293 K	0.21	0.29	3.19	5.84
ε' at 500 MHz	3.94	3.29	3.41	4.10
ε' at 2 GHz	3.84	3.19	3.24	3.41
Tan $\delta \times 10^{-3}$ at 500 MHz	11.0	8.0	26.0	15.0
Tan $\delta \times 10^{-3}$ at 2 GHz	13.0	4.6	5.7	60.0

heat-treatment temperature. This depends on sintering conditions—the higher the sintering temperature the greater the grain size. During the sintering of hexaferrite samples, grain growth occurs via diffusion of constituent ions in the ferrite lattices. The ion diffusion coefficient can be expressed by use of the relationship $\eta = \eta_o \exp(-\beta/T)$ (where η_o and β are constants and T is the sintering temperature).[18] The diffusion coefficient increases gradually with increasing sintering temperature, so crystallite size increases. Samples with crystallite size less than 50 nm can be useful for high-density recording media.[19]

The density was calculated by use of the relationship:

$$d_m = \frac{m}{\pi r^2 h}, \quad (2)$$

where mass of the pellet is m, the radius of the pellet is r, and the thickness of the pellet is h. The density of synthesized hexaferrite samples increased in the range 4.25–4.51 g cm^{-3}, which may be attributed to increasing particle size with increasing heat-treatment temperature from 700°C to 900°C, as shown in Table I. Sample density decreased after treatment at 1000°C, which is attributed to the presence of pores created during heat treatment because of the higher temperature. Variation of bonding in the M-type hexaferrite structure occurred because of the creation of pores. The porosity of the samples decreased; this explains the increase in density, because of increase of particle size with increasing heat-treatment temperature.[20]

Figure 4 shows the SEM pattern of a sample of M-type barium hexaferrite $BaCr_xGa_xFe_{12-2x}O_{19}$ (x = 0.2) powder heat treated at 1000°C. No significant information appeared in the SEM patterns of samples heat treated at 700°C, 800°C, and 900°C, but some grains become visible in the SEM pattern of the sample heat treated at 1000°C. Fang et al.[21] and Jacobo et al.[22] reported that average crystallite size determined by use of the Scherrer formula was smaller than the average grain size derived from SEM measurements. This may be because of aggregation of a large number of crystallites.[11]

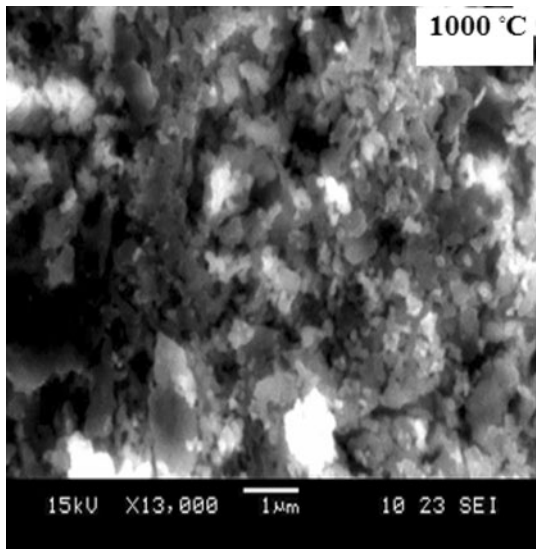

Fig. 4. SEM pattern of single phase M-type hexaferrite $BaCr_xGa_xFe_{12-2x}O_{19}$ (x = 0.2) powder heat treated at 1000°C.

Elemental analysis of the powder sample was performed by use of the EDXS. The analysis also determined the weight percent of elements detected in the compound. Figure 5 shows an EDXS spectrum of a sample of Cr–Ga-substituted single phase M-type barium hexaferrite $BaCr_xGa_xFe_{12-2x}O_{19}$ (x = 0.2) powder heat treated at 1000°C.

The labeled peaks in the spectrum confirm the presence of dissolved elements Ba, Fe, Ga, and Cr in the compound. The weight percent of the elements is given as:

Ba	Fe	Cr	Ga	Total
18.61	79.15	1.13	1.11	100

Oxygen and carbon content were not included in the EDXS analysis, because lower atomic number elements cannot be measured accurately by EDXS analysis.[11]

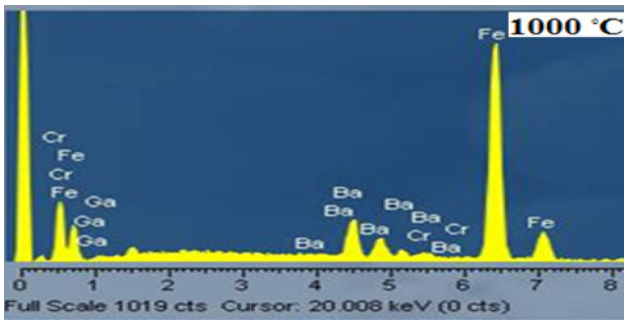

Fig. 5. EDXS spectrum of single phase M-type hexaferrite $BaCr_xGa_xFe_{12-2x}O_{19}$ ($x = 0.2$) powder heat treated at 1000°C.

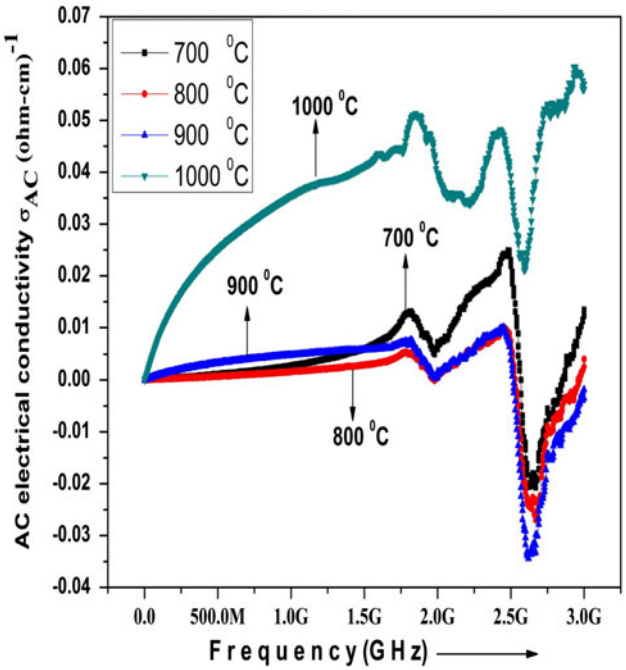

Fig. 6. Dependence of AC electrical conductivity (σ_{AC}) on applied field frequency and on heat-treatment temperature (700°C, 800°C, 900°C, and 1000°C).

Electrical Properties

Frequency-Dependent AC Electrical Conductivity (σ_{AC})

Figure 6 shows the variation of AC electrical conductivity (σ_{AC}) in the high-frequency range (1 MHz–3 GHz).

The AC conductivity results can be explained on the basis of the assumption that real AC conductivity consists of two parts:[23]

$$\sigma' = \sigma_{DC} + \sigma_{AC}. \quad (3)$$

The first term, σ_{DC}, is the DC conductivity, which is frequency-independent and can be written as:

$$\sigma_{DC} = \sigma_0 \exp(-E/kT), \quad (4)$$

where E is the activation energy for electrical conduction, σ_0 is a pre-exponential constant, and k is Boltzmann's constant. The second term σ_{AC} is temperature and frequency-dependent and is given as:[23,24]

$$\sigma_{AC} = B(T)\omega^n(T), \quad (5)$$

where B has units of conductivity (Ω^{-1} cm^{-1}) and n is a dimensionless exponent and depends on composition and temperature, $\omega = 2\pi f$ is the angular frequency. The AC electrical conductivity (σ_{AC}) of the synthesized samples was calculated from dielectric data by use of the relationship:

$$\sigma_{AC} = \omega\varepsilon_0\varepsilon'' = \omega\varepsilon_0\varepsilon'\tan\delta, \quad (6)$$

where $\omega = 2\pi f$ represents the angular frequency and ε_0 indicates the permittivity of free space. The ac conductivity (σ_{ac}) of ferrites depends on the hopping of electrons between Fe^{3+} and Fe^{2+} ions in the octahedral sites. The ac conductivity (σ_{ac}) gradually increases with increasing frequency of the applied ac field. The frequency of electron hopping between charge carriers Fe^{3+} and Fe^{2+} increases with increasing applied field frequency and hence ac conductivity (σ_{ac}) increases. In ferrites both the hopping of charge carriers and charge liberated are significant in the mechanism of conduction.[25] According to the Maxwell–Wagner model and Koops phenomenological theory, ferrite materials consist of conducting grains separated by highly resistive thin layers of grain boundaries. The results for ac conductivity (σ_{ac}) at low frequencies show the grain boundary behavior, but the dispersion behavior at high frequencies may be because of the conducting nature of grains.[26]

Heat-Treatment Temperature-Dependent AC Electrical Conductivity (σ_{AC})

Figure 6 also shows the variation of AC electrical conductivity (σ_{AC}) for samples heat treated at 700°C, 800°C, 900°C, and 1000°C. AC conductivity (σ_{AC}) is enhanced by increasing the heat-treatment temperature. The AC conductivity reached its highest value, 27.0×10^{-3} Ω cm^{-1}, for the sample heat treated at 1000°C. The increase in AC conductivity depends on the amount of Fe^{2+} ions formed because of the partial decrease of Fe^{3+} ions during the heat-treatment process. The Fe^{2+} ion content is a characteristic property of a ferrite material. Its value depends on different factors such as heat-treatment temperature, heat-treatment time, and heat-treatment atmosphere, etc. The increase in AC conductivity is attributed to the formation of excess Fe^{2+} ions with increasing heat-treatment temperature. Table I shows the heat-treatment temperature-dependent values of AC conductivity at a frequency of 500 MHz.

Heat-Treatment Temperature-Dependent DC Electrical Resistivity

The DC electrical resistivity of samples heat treated at 700°C, 800°C, 900°C, and 1000°C was measured by use of the two-probe method at room temperature. The DC resistivity was calculated by use of the relationship:

$$\rho = \frac{RA}{h}, \tag{7}$$

where R is the resistance, h the thickness, and A (πr^2) the area of pellet sample.

Figure 7 shows the variation of room temperature DC electrical resistivity for samples heat treated at 700°C, 800°C, 900°C, and 1000°C. The resistivity increased from 0.21×10^9 Ω cm to 5.84×10^9 Ω cm with increasing heat-treatment temperature. Conduction in ferrites is because of the hopping of electrons from Fe^{3+} to Fe^{2+} ions at the octahedral sites i.e. Fe^{3+}–O–Fe^{2+}.[27,28] The number of pores is small after treatment at lower temperatures, and these result in less hindrance of the hopping of charge carriers between ferric Fe^{3+} and ferrous Fe^{2+} ions; the resistivity of these ferrites is therefore smaller. At higher temperature, the number of pores increases, which results in more hindrance of the hopping of charge carriers [20], hence resistivity is enhanced with increasing heat-treatment temperature.

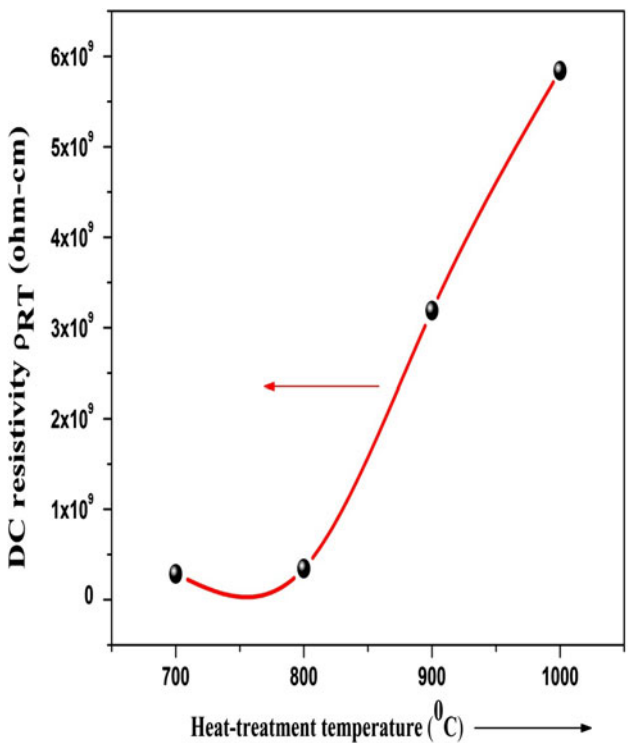

Fig. 7. DC electrical resistivity of M-type hexaferrite $BaCr_xGa_xFe_{12-2x}O_{19}$ ($x = 0.2$) heat treated at 700°C, 800°C, 900°C, and 1000°C.

The main effect of the non-magnetic impurity phase (α-Fe_2O_3) is to isolate the hexaferrite particles from each other and thus reduce the interaction between them; this is known to have a detrimental effect on the properties of the materials. Re-adjustment of M-type hexaferrite phase structure and elimination of defects occur during the heat treatment. Evolution of the structure of the M-type hexaferrite phase is responsible for changes in the electrical properties. The following reactions occur during the formation of M-type barium hexaferrite ($BaFe_{12}O_{19}$) from barium oxide and ferric oxide:[29]

$$BaO + Fe_2O_3 = BaFe_2O_4, \tag{8}$$

$$BaO + 6Fe_2O_3 = BaFe_{12}O_{19}, \tag{9}$$

$$BaFe_2O_4 + 5Fe_2O_3 = BaFe_{12}O_{19}. \tag{10}$$

The charge carriers are thermally activated because of increase in the heat-treatment temperature. As the temperature increases, the percentage of the M-type hexaferrite phase increased and the amount of impurity phase (α-Fe_2O_3) decreased, because of its elimination. The cations combined with anions because of the increase in the heat-treatment temperature. The single phase M-type hexaferrite was obtained after heat treatment at 1000°C and at this stage all cations thermally combined with anions. After heat treatment at 1000°C, the impurity phase (α-Fe_2O_3) was completely eliminated and the M-type hexaferrite phase was maximum.[16] Therefore, conduction of charge carriers between ferric Fe^{3+} and ferrous Fe^{2+} ions decreased with the increasing heat-treatment temperature and, as a result, the DC resistivity of these ferrite materials was enhanced. The synthesized materials can be useful for MLCI applications because of enhanced DC resistivity 5.84×10^9 Ω cm, i.e. higher than 10^8 Ω cm.[30] The materials can also be useful for reducing eddy current losses at higher frequencies because of high resistivity.

High-Frequency Dielectric Measurements

Dielectric Constant (ε′)

The dielectric properties of ferrite materials mainly depend on their physical and chemical properties, as a result of different polarization phenomena. Figure 8 shows dielectric constant as a function of frequency in the range 1 MHz–3 GHz. It is observed that the frequency and heat-treatment temperature significantly affect on the dielectric constant for all samples; however, the dielectric constant is high for all samples at low frequencies and decreases or becomes independent of increasing frequency from 1 MHz to 3 GHz.[31] The dielectric properties of polycrystalline ferrite materials arise

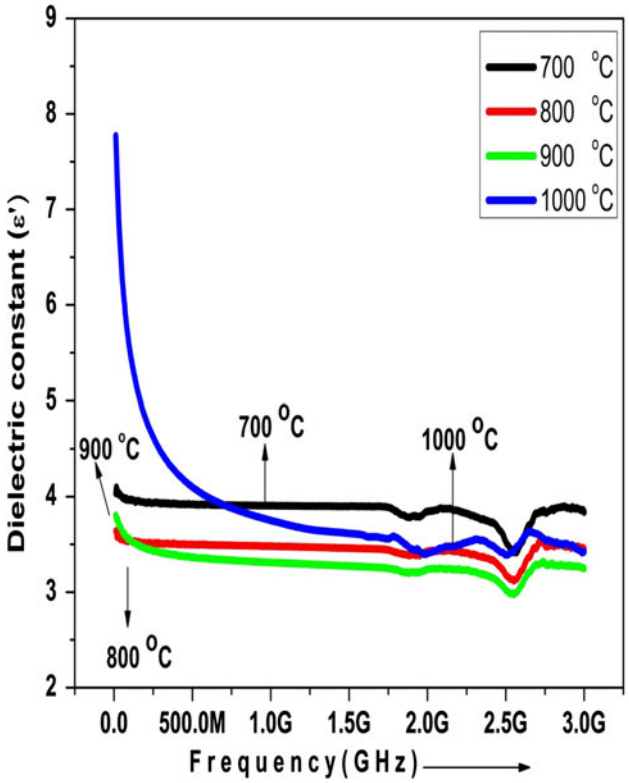

Fig. 8. Variation of dielectric constant (ε') with applied field frequency and heat-treatment temperature (700°C, 800°C, 900°C, and 1000°C).

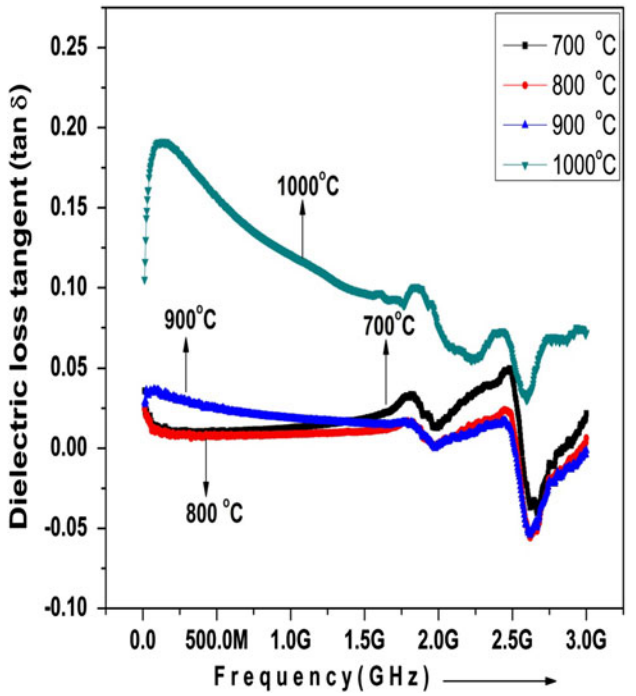

Fig. 9. Variation of dielectric loss tangent (tan δ) versus applied field frequency and heat-treatment temperature (700°C, 800°C, 900°C, and 1000°C).

because of interfacial polarization; this results from the heterogeneous structure of ferrites, which consist of low-resistivity grains separated by higher-resistivity grain boundaries as elaborated by Koop's phenomenological theory.[32] The decrease in dielectric constant for all the samples heat treated at different temperatures with increasing frequency is because the polarization decreases with increasing frequency and then becomes constant.[33] The mechanism of polarization in ferrites is similar to that of conduction. Electron exchange between Fe^{2+} and Fe^{3+} on octahedral 2a crystallographic sites results in local displacement of electrons in the direction of the applied field, which determines the polarization.[34,35] Polarization reduces with increasing applied field frequency and then becomes constant, which may be because electron exchange between Fe^{2+} and Fe^{3+} cannot follow the alternating field beyond a specific applied field external frequency.[36] Heat-treatment temperature-dependent values of dielectric loss tangent at frequencies of 500 MHz and 2 GHz are shown in Table I.

Dielectric Loss Tangent (Tan δ)

Figure 9 shows the dielectric loss, which decreases with increasing applied electric field frequency, for hexaferrite materials heat treated at different temperatures. The observed trend can be explained on the basis of Koop's theory [32] which is based on the Maxwell–Wagner model for the inhomogeneous double-layer structure of dielectric materials. The dielectric structure is supposed to be composed of fairly well conducting ferrite grains separated by the thin, poorly conducting grain boundaries. These grain boundaries could be created during the heat-treatment process because of superficial reduction or oxidation of crystallites in the porous materials as a result of their direct contact with the firing atmosphere.[37] The grain boundaries of lower conductivity were observed to be effective at lower frequencies whereas ferrite grains of high conductivity were effective at high frequencies.[38,39] This explains the greater dielectric loss at lower applied electric field frequency and the decreasing trend as the applied electric field frequency increases; at higher frequency it becomes independent of applied field frequency because electron exchange between Fe^{2+} and Fe^{3+} cannot follow the alternating field. Figure 9 clearly shows the appearance of resonance peaks in the profiles of dielectric loss tangent (tan δ) for all the samples at frequencies of approximately 1.8 GHz and 2.5 GHz. The peaks appear when the frequency of jumping of electrons between Fe^{2+} and Fe^{3+} is equal to the frequency of the applied ac field and as a result resonance occurs.[40,41] When the frequency of the external applied ac field is equal to the natural frequency of ions, maximum electrical energy is transferred to the oscillating ions and the power loss

increases substantially. As a result, the phenomenon of resonance occurs and the resonance peaks appeared.[42] Moreover, the position of peaks shifts toward the lower frequency region with increasing Cr–Ga contents. The low-frequency dislocation of the relaxation peak may represent the region of frequencies in which ions can perform successful hopping from one site to the neighboring site. The higher frequency peak may indicate the range of frequencies in which the ions are confined to their potential wells and can make localized motion within the well.[43] The heat-treatment temperature-dependent values of dielectric loss tangent at frequencies of 500 MHz and 2 GHz are shown in Table I.

Dielectric Dissipation Factor (ε″)

The dielectric dissipation factor is the product of dielectric loss tangent (tan δ) and dielectric constant (ε) as given by the relationship $\varepsilon'' = \varepsilon \tan \delta$.[27] When an oscillating electric field is applied, the dissipation factor gives the magnitude of energy dissipated in a dielectric. Figure 10 shows the profile of dielectric dissipation factor versus applied frequency. It is observed that its value decreases with increasing frequency. The dissipation factor directly depends on the value of the loss tangent. The polarization response lags behind the frequency as the frequency of applied field approaches the relaxation frequency. The internal frictional forces hindered the movement of each dipole, which leads to heating in the sample, and power loss. The power loss in dielectric materials may be because of work done to overcome the frictional damping forces acting on each dipole during their rotation. The dielectric loss is an essential part of the total core loss in hexaferrites. This power loss may be significant at applied field frequencies near the relaxation frequencies for each dipole in a particular dielectric material.[28] Hence, low dielectric dissipation is desirable for low core loss. The resonance peaks appeared for all the samples in the profiles of dielectric loss tangent (tan δ) at frequencies of approximately 1.8 GHz and 2.5 GHz, as shown in Fig. 10. The peaks appear when the frequency of jumping of electrons between Fe^{2+} and Fe^{3+} is equal to the frequency of the applied ac field and as a result resonance occurs.[40,41]

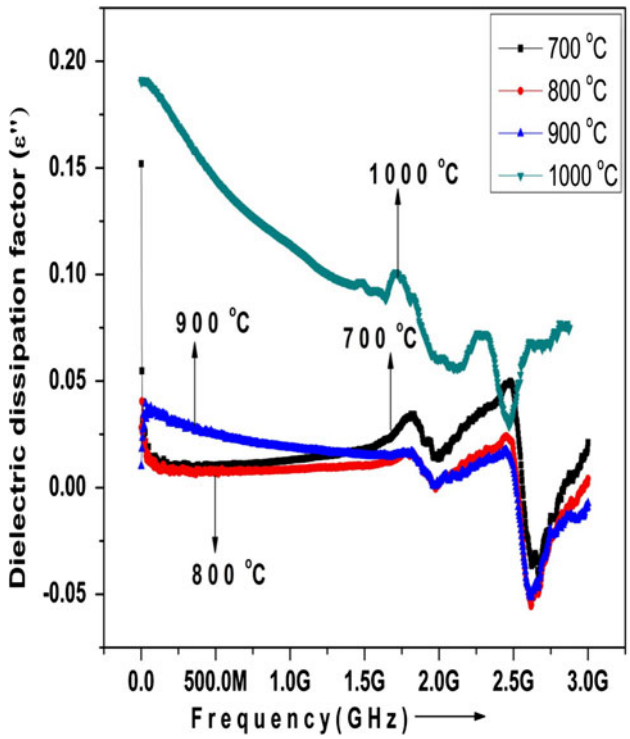

Fig. 10. Variation of dielectric dissipation factor (ε″) versus applied field frequency and heat-treatment temperature (700°C, 800°C, 900°C, and 1000°C).

Impedance (Z)

Figures 11 and 12 show, respectively, the variation of the real (Z') and imaginary (Z'') parts of impedance at room temperature as a function of frequency from 1 MHz to 3 GHz). Figure 11 shows the variation of the real part (Z') for a sample heat treated at 1000°C. For all the samples, the values of both real and imaginary parts of impedance are higher at low frequencies and decrease with increasing applied field frequency from 1 MHz to 3 GHz.[44] It is observed that both real and imaginary parts of impedance indicate the possibility of an

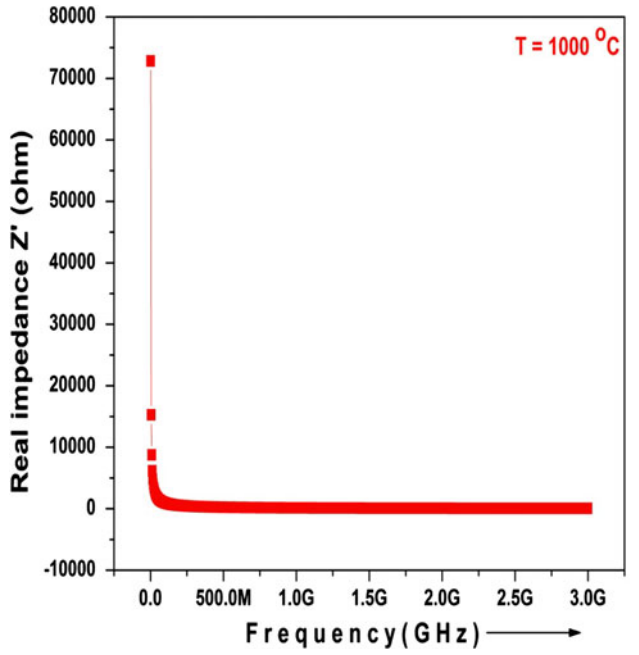

Fig. 11. Variation of the real part of impedance (Z') versus applied field frequency for a sample heat treated at 1000°C.

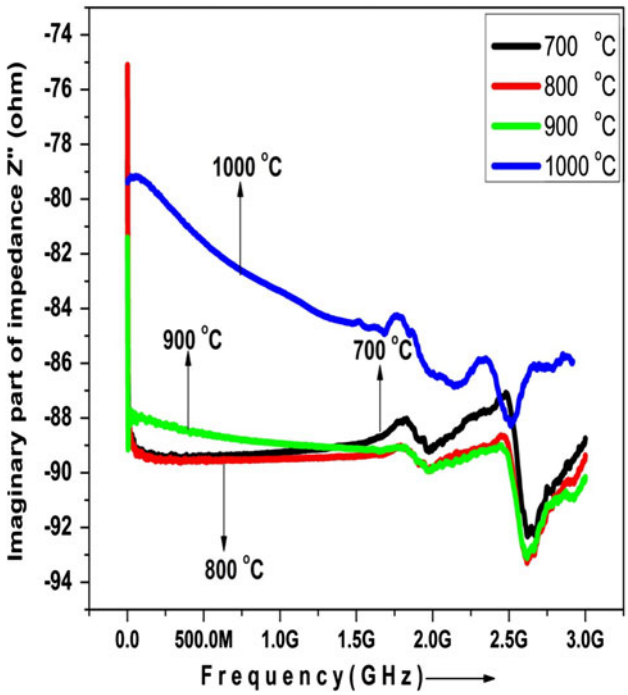

Fig. 12. Variation of the imaginary part of impedance (Z'') versus applied field frequency and heat-treatment temperature (700°C, 800°C, 900°C, and 1000°C).

increase in AC conductivity with increasing applied field frequency. The impedance in the higher-frequency region suggests a possible release of space charge and reduction of the barrier properties of the materials. Both real and complex parts of impedance become almost independent of frequency in the higher-frequency region.[45,46] Figure 12 clearly shows that some peaks appeared in the profile of imaginary part of impedance at frequencies of approximately 1.8 GHz and 2.5 GHz.[40,41]

CONCLUSIONS

M-type hexaferrite $BaCr_xGa_xFe_{12-2x}O_{19}$ ($x = 0.2$) powders have been prepared by sol–gel autocombustion, a simple and economical method. XRD analysis reveals formation of the pure M-type hexagonal phase, with average crystallite size in the range 44–73 nm, in samples heat treated at 1000°C. The DC resistivity increases from 0.21×10^9 Ω cm to 5.84×10^9 Ω cm with increasing heat-treatment temperature. The dielectric constant and dielectric loss tangent decrease and AC conductivity increases with increasing applied field frequency. Resonance peaks appear in the profiles of different properties, for example AC conductivity, dielectric loss tangent, dielectric dissipation factor, and complex impedance. Owing to these qualities, the synthesized single-phase materials might be useful for high-frequency applications to reduce eddy current losses and radar absorbing waves.

REFERENCES

1. A.M. Abo El Ata, M.K. El Nimr, D. El Kony, and A.H. AL-Hammad, *J. Magn. Magn. Mater.* 204, 36 (1999).
2. A. Kale, S. Gubbala, and R.D.K. Misara, *J. Magn. Magn. Mater.* 277, 350 (2004).
3. C. Kittle, *Phys. Rev.* 70, 965 (1946).
4. C.A. Stergiou, I. Manolakis, T.V. Yioultsis, and G. Litsardakis, *J. Magn. Magn. Mater.* 322, 1532 (2010).
5. H. Kojima, *Ferromagnetic Materials*, Vol. 3, ed. E.P. Wohlfarth (Amsterdam: North-Holland Publishing Company, 1982), p. 305.
6. L. Junliang, Z. Yanwei, G. Cuijing, Z. Wei, and Y. Xiaowei, *J. Eur. Ceram. Soc.* 30, 993 (2010).
7. N. Rezlescu, C. Doroftei, E. Rezlescu, and P.D. Popa, *J. Alloys Compd.* 451, 492 (2008).
8. S. Ounnunkada and P. Winotai, *J. Magn. Magn. Mater.* 301, 292 (2006).
9. I. Bsoul and S.H. Mahmood, *J. Alloys Compd.* 489, 110 (2010).
10. I. Ali, M.U. Islam, M.S. Awan, and M. Ahmad, *J. Alloys Compd.* 547, 118 (2013).
11. I. Ali, M.U. Islam, M.S. Awan, and M. Ahmad, *J. Mater. Eng. Perform.* (2013). doi:10.1007/s11665-013-0484-4.
12. I. Ali, M.U. Islam, M.S. Awan, M. Ahmad, M.N. Ashiq, and S. Naseem, *J. Alloys Compd.* 550, 564 (2013).
13. K.K. Mallick, P. Shepherd, and R.J. Green, *J. Eur. Ceram. Soc.* 27, 2045 (2007).
14. A. Mali and A. Ataie, *Scripta Mater.* 53, 1066 (2005).
15. P. Shepherd, K.K. Mallick, and R.J. Green, *J. Magn. Magn. Mater.* 311, 683 (2007).
16. J.F. Wang, C.B. Ponton, and I.R. Harris, *J. Alloys Compd.* 403, 104 (2005).
17. W. Yongfei, L. Qiaoling, Z. Cunrui, and J. Hongxia, *J. Alloys Compd.* 467, 284 (2009).
18. H. Sim, J.M. Xue, and J. Wang, *Mater. Lett.* 58, 2032 (2004).
19. S. Che, J. Wang, and Q. Chen, *J. Phys. Condens. Mater.* 15, L335 (2003).
20. M. Ahmad, I. Ali, F. Aen, M.U. Islam, M.N. Ashiq, S. Atiq, W. Ahmad, and M.U. Rana, *Ceram. Int.* 38, 1267 (2012).
21. H.C. Fang, Z. Yang, C.K. Ong, Y. Lie, and C.S. Wang, *J. Magn. Magn. Mater.* 187, 129 (1998).
22. S.E. Jacobo, L. Civali, and M.A. Blesa, *J. Magn. Magn. Mater.* 37, 260 (2003).
23. A.K. Jonscher, *Dielectric Relaxation in Solids* (London: Chelsea Dielectric Press, 1983).
24. M.F. Mostafa, M.M. Abd. El Kader, A.S. Atallah, and M.K. El Nimr, *Phys. Status Solidi A* 135, 549 (1993).
25. K.M. Batoo, S. Kumar, C.G. Lee, and Alimuddin, *J. Curr. Appl. Phys.* 9, 826 (2009).
26. K.C. Kao, *Dielectric Phenomena in Solids, Ch. 2* (San Diego, CA: Elsevier Academic Press, 2004), p. 51.
27. N. Gupta, M.C. Dimri, S.C. Kashyap, and D.C. Dube, *Ceram. Int.* 31, 171 (2005).
28. M.N. Ashiq, M.J. Iqbal, and I.H. Gul, *J. Alloys Compd.* 487, 341 (2009).
29. J. Huang, H. Zhuang, and W.L. Li, *Mater. Res. Bull.* 38, 149 (2003).
30. L. Jia, J. Luo, H. Zhang, G. Xue, and Y. Jing, *J. Alloys Compd.* 489, 162 (2010).
31. Y.P. Wu, C.K. Ong, Z.W. Li, L. Chen, and G.Q. Lin, *J. Appl. Phys.* 97, 063909 (2005).
32. C.G. Koops, *Phys. Rev.* 83, 121 (1951).
33. A.M. Shaikh, S.S. Bellard, and B.K. Chougule, *J. Magn. Magn. Mater.* 195, 384 (1999).
34. I.T. Rabinkin and Z.I. Novikova, *Ferrites* (Minsk: Izv Acad, Nauk USSR, 1960), p. 146.
35. S.B. Narang and I.S. Hudiara, *J. Ceram. Process. Res.* 7, 113 (2006).
36. R.G. Kharabe, R.S. Devan, C.M. Kanamadi, and B.K. Chougule, *Smart Mater. Struct.* 15, N36 (2006).
37. P.V. Reddy, T.S. Rao, and J. Less, *Common Metals* 86, 255 (1982).

38. B.K. Kunar and G.P. Srivastava, *J. Appl. Phys.* 75, 6115 (1994).
39. M.A. El Hiti, *J. Magn. Magn. Mater.* 192, 305 (1999).
40. M.B. Reddy and P.V. Reddy, *Appl. Phys. (UK)* 24, 975 (1991).
41. S.C. Watawe, B.D. Sarwede, S.S. Bellad, B.D. Sutar, and B.K. Chougule, *J. Magn. Magn. Mater.* 214, 55 (2000).
42. S.S. Bellad and B.K. Chougule, *Mater. Chem. Phys.* 66, 58 (2000).
43. K.P. Padmasree, D.K. Kanchan, and A.R. Kulkarni, *Solid State Ion.* 177, 475 (2006).
44. M.J. Iqbal, M.N. Ashiq, and I.H. Gul, *J. Magn. Magn. Mater.* 322, 1720 (2010).
45. R.S. Devan, Y.R. Ma, and B.K. Chougule, *Mater. Chem. Phys.* 115, 263 (2009).
46. A. Kumar, B.P. Singh, R.N. Choudhary, P. Awalendra, and K. Thakur, *Mater. Chem. Phys.* 99, 150 (2006).